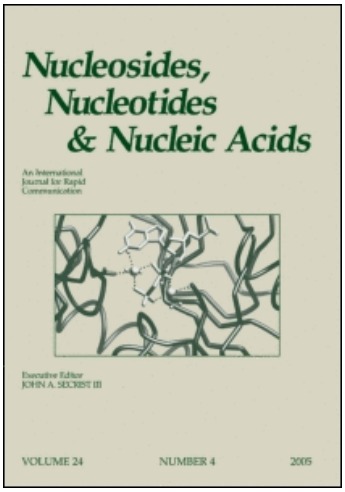

Nucleosides, Nucleotides and Nucleic Acids

Publication details, including instructions for authors and subscription information:
http://www.informaworld.com/smpp/title~content=t713597286

Structure of the Biologically Relevant G-Quadruplex in The c-MYC Promoter

Danzhou Yang[ab]; Laurence H. Hurley[abcd]

[a] College of Pharmacy, University of Arizona, Tucson, Arizona, USA [b] Arizona Cancer Center, Tucson, Arizona, USA [c] Department of Chemistry, University of Arizona, Tucson, Arizona, USA [d] B105 Collaborative Institute, University of Arizona, Tucson, Arizona, USA

To cite this Article Yang, Danzhou and Hurley, Laurence H.(2006) 'Structure of the Biologically Relevant G-Quadruplex in The c-MYC Promoter', Nucleosides, Nucleotides and Nucleic Acids, 25: 8, 951 — 968

To link to this Article: DOI: 10.1080/15257770600809913

URL: http://dx.doi.org/10.1080/15257770600809913

Nucleosides, Nucleotides, and Nucleic Acids, 25:951–968, 2006

ISSN: 1525-7770 print / 1532-2335 online
DOI: 10.1080/15257770600809913

Taylor & Francis
Taylor & Francis Group

STRUCTURE OF THE BIOLOGICALLY RELEVANT G-QUADRUPLEX IN THE c-MYC PROMOTER

Danzhou Yang □ *University of Arizona, College of Pharmacy, Tucson, Arizona, USA; Arizona Cancer Center, Tucson, Arizona, USA*

Laurence H. Hurley □ *University of Arizona, College of Pharmacy, Tucson, Arizona, USA; Arizona Cancer Center, Tucson, Arizona, USA; University of Arizona, Department of Chemistry, Tucson, Arizona, USA; B105 Collaborative Institute, University of Arizona, Tucson, Arizona, USA*

□ *The nuclease hypersensitivity element III_1 (NHE III_1) in the c-MYC promoter controls up to 80–90% of the transcriptional activity of this gene. We have demonstrated that the guanine-rich strand of the NHE III_1 forms a G-quadruplex consisting of a mixture of four biologically relevant loop isomers that function as a silencer element. NMR studies have shown that these G-quadruplexes are propeller-type parallel structures consisting of three stacked G-tetrads and three double-chain reversal loops. An NMR-derived solution structure for this quadruplex provides insight into the unusual stability of the structure. This structure is a target for small molecule inhibitors of c-MYC gene expression.*

Keywords c-MYC; G-quadruplex; Transcriptional control

INTRODUCTION

Expression of the c-MYC oncogene is linked to potentiation of cellular proliferation and to inhibition of differentiation, leading to its association with a number of human and animal malignancies, including carcinomas of the breast, colon, and cervix, as well as small-cell lung cancer, osteosarcomas, glioblastomas, and myeloid leukemias.[1–4] Simply blocking c-MYC expression with antisense oligonucleotides has been shown to induce differentiation of myelocytes and myeloid leukemia cells, further cementing the inverse relationship between expression of this oncogene and differentiation.[5–7] In transfection experiments, c-MYC was demonstrated

Received 2 May 2005; accepted 16 May 2005.
Presented at the XVI International Roundtable, September 12–16, 2004, Minneapolis, Minnesota.
Address correspondence to Laurence H. Hurley, University of Arizona, College of Pharmacy, 1703 E. Mabel, Tucson, AZ 85721. E-mail: hurley@pharmacy.arizona.edu

to immortalize normal fibroblasts, and in concert with a cooperating oncogene such as v-ABL or v-RAS, it causes malignant transformation.[4] Much of this activity stems from the ability of c-MYC to act as both a transcriptional activator and repressor, inducing genes involved in proliferation, such as CAD, CDC25A, ODC, and hTERT, and repressing genes involved in growth arrest, such as GADD45.[4] It has also been found that c-MYC plays a role in the apoptotic response.[1,4,8] Significantly, it has been recently demonstrated that even transient downregulation of c-MYC results in apoptosis in a highly malignant osteogenic sarcoma.[9] For all of these reasons, c-MYC has emerged as an attractive target for anti-cancer therapeutic agents.

The NHE III_1 in the c-MYC Promoter Forms an Intramolecular Parallel G-Quadruplex Structure

The NHE III_1 of the c-MYC promoter controls 80–90% of c-MYC transcription and has been the subject of considerable research over the past two decades.[10–20] The NHE III_1 is a 27-base-pair sequence, located –142 to –115 base pairs upstream of the P1 promoter (Figure 1). This duplex element can equilibrate between transcriptionally active forms (duplex and single-stranded DNA) and a silenced form.[21] We have previously shown that single G-to-A mutations, which destabilize the G-quadruplex forming unit, result in a threefold increase in basal transcriptional activity (see later).[22] In contrast, agents that stabilize the specific G-quadruplex structure are able to suppress c-MYC transcriptional activity.[22] Furthermore, on the basis of DMS footprinting, we had proposed a model in which the biologically relevant structure was a chair G-quadruplex.[22] This conclusion was based upon similar proposals for structures of the HIV aptamer T30695 and the thrombin binding aptamer (TBA).[23–26] The chair structure of TBA was proposed on the basis of NMR[23] and X-ray crystallography,[27] while the chair structure of T30695 was proposed only on the basis of

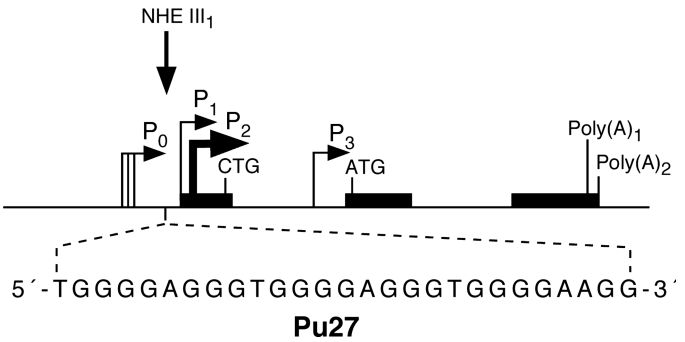

FIGURE 1 Promoter structure of the c-MYC gene; shown in the inset is the 27-mer sequence of the purine-rich strand upstream of the P1 promoter.[3]

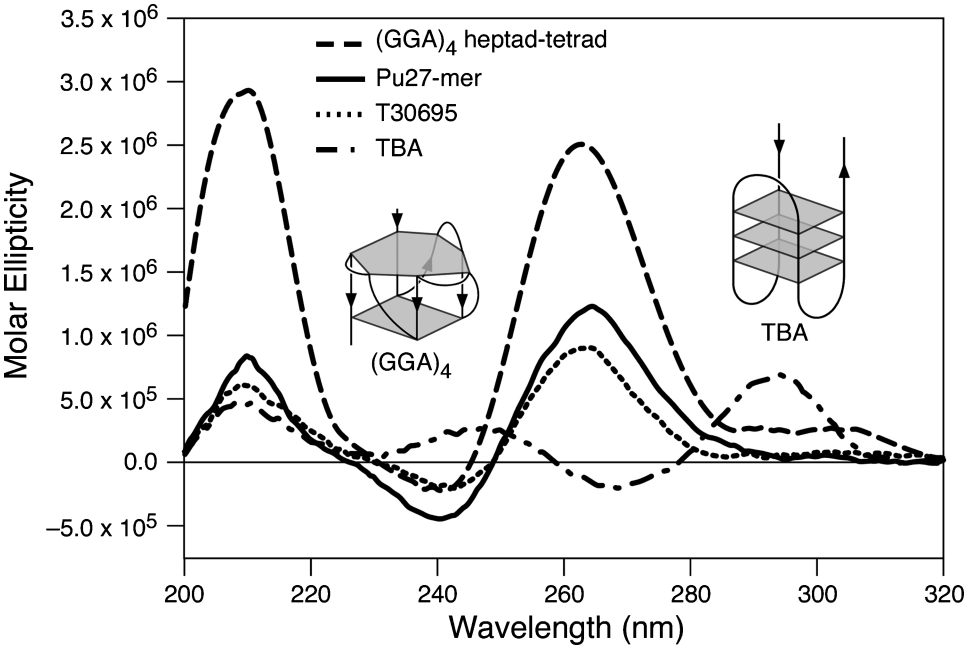

FIGURE 2 (A) CD spectra of the d(GGA)$_4$ oligonucleotide, the Pu27-mer, the T30695 oligonucleotide, and the thrombin binding aptamer (TBA). All CD data were obtained with a 10 μM strand concentration in the presence of 100 μM KCl at 25°C.

NMR studies.[26] However, upon examination by CD it was found that while the spectra of T30695 and the Pu27-mer were coincident, the TBA gave a very different CD signature;[28] i.e., the T30695 and Pu27-mer showed absorption maxima at 262 nm, while the TBA had a maxima at 295 nm (Figure 2). Only the CD of the TBA is in accordance with an antiparallel structure,[29] while the CD signatures of the T30695 and the c-MYC Pu27-mer are consistent with a parallel structure,[29,30] which is typified by the heptad-tetrad structure determined previously by NMR[31,32] and shown in Figure 2. Therefore, we conclude that the NHE III$_1$ in the c-MYC promoter forms an intramolecular parallel G-quadruplex structure, and the HIV aptamer T30695 also most likely has a similar folding pattern.

Only the Four Consecutive 3′ Runs of Guanines Are Involved in G-Tetrad Formation, and within These 3′ Runs, G11, G14, G20, and G23 Are Less Critical for G-Quadruplex Stability

The availability of N7 of guanine for methylation by DMS in duplex and single-stranded DNA, but not in G-tetrads, is a diagnostic indicator of G-quadruplex structures. In the previously reported DMS-induced cleavage experiment,[22] within the four consecutive 3′ runs of guanines, only G11,

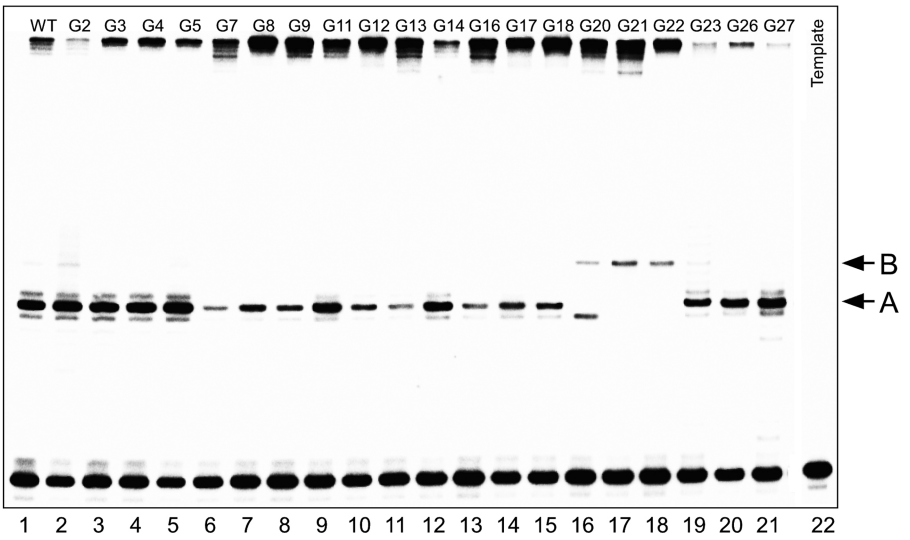

FIGURE 3 Effect of single G-to-A mutations at positions G2–G27 (lanes 2–21) on the stability of the Pu27-mer sequence in the polymerase stop assay.[22] Each of these lanes contained the mutant oligomer incubated with Taq polymerase at 37°C (10 mM KCl and NaCl). Lane 22 lacked Taq polymerase. Arrows A and B refer to the polymerase stop products corresponding to either the four 3′ runs of guanines (A) or four 5′ runs of guanines (B).

G14, G20, and G23 showed cleavage, suggesting that they were not involved in stable G-tetrad formation. If these guanines are not involved in the G-tetrads, then mutation to adenines should not significantly affect G-quadruplex stabilization. A polymerase stop assay was used to evaluate the effect of single guanine mutations (G to A) on G-quadruplex stability.[28] The results (Figure 3) show that the 5′ run of guanines (G2–G5) is not required for formation of a stable G-quadruplex structure, as predicted from the DMS cleavage results.[22] However, for the four consecutive 3′ runs of guanines, the pattern is more complex. G7–G9, G12–G13, G16–G18, and G21–G22 are clearly critical for G-quadruplex stability, while G11, G14, G23, and, perhaps, G20 appear less critical. The upper band (B in Figure 3) for the G-to-A mutations at G20, G21, and G22 corresponds to a new polymerase stop site that presumably results from an alternative structure that uses the four consecutive 5′ runs of guanines. The G20 mutation is unique in that it shows that both types of G-quadruplex structures can be formed using either the four consecutive 5′ or 3′ runs of guanines. The lack of dependency on G11, G14, and G23—and perhaps G20—for G-quadruplex stability can be explained if we assume a degeneracy in use of the two runs of four guanines (i.e., G11–G14 and G20–G23), such that only three of the four guanines are required in each case. It should be noted that the other two consecutive 3′ runs of guanines (G7–G9 and G16–G18) have only three guanines, not allowing for degeneracy in these cases.

A Parallel G-Quadruplex Structure for the Pu18-Mer Is Compatible with Four Different Loop Isomers

The four possible loop isomers of the Pu18-mer parallel structure are shown in the upper row of structures in Figure 4A. These three-tetrad-containing loop isomers result from the degeneracy of the two runs of four guanines (G11–G14 and G20–G23), such that guanine slippage can occur so that either G11 or G14 (or G20 or G23) is involved in tetrad formation, while the other guanine is located within a loop. In order to eliminate this degeneracy, four different dual G-to-T mutations in the 18-mer were designed and synthesized (G→T-14,23, -14,20, -11,23, -11,20) so that each of the two runs of four guanines is reduced to three, and the resulting mutant thymines are forced to assume loop positions in order to preserve the three tetrad structures (lower row of structures in Figure 4A). The wild-type Pu18-mer sequence and the four dual mutants were subjected to an electromobility shift assay (EMSA), and the results are shown in Figure 4B. The wild-type sequence (lane 1) shows two bands, while each of the four different dual mutants shows only one band (lanes 2–5). On the basis of a comparison of the mobility of the bands corresponding to the wild-type and the four mutant 18-mers, band B in the wild-type sequence corresponds to loop isomers where G23 is intratetrad, while for band A, G23 is external. DMS footprinting of these four different dual mutants failed to show any cleavage, which indicates that for each 18-mer all of the guanines are involved in formation of G-tetrads (unpublished results).

Finally, each of the dual mutant loop isomers has a significantly lower melting temperature than the wild-type sequence.[28] The T_m value of each of the four loop isomers (A–D in Figure 4A) was determined by CD under the same conditions described for the Pu27-mer, and all the values were found to be between 68 and 72°C.

The 1:2:1 Loop Isomer Is the Predominant Isomer in the Mixture

With the loop isomers having been defined through the dual-mutant studies, it was now possible to reconstruct in the wild-type sequence the dynamic state of individual guanines that can interchange between loop and tetrad positions. Thus, G11, G14, G20, and G23 can either be within a loop (cleavage by DMS) or part of a G-tetrad structure (no DMS cleavage). This explains the only partial protection of certain guanines in the Pu27-mer sequence following DMS cleavage[22] and, conversely, the ability of the four dual mutants to form separate, defined G-quadruplex structures. It is unlikely that all four isomers occur in equal proportions. The pronounced DMS cleavage of G14 and G23 suggests that these guanines are either within the loops (G14) or external to the quadruplex (G23), and therefore the A loop isomer shown in Figure 4A is probably predominant within the

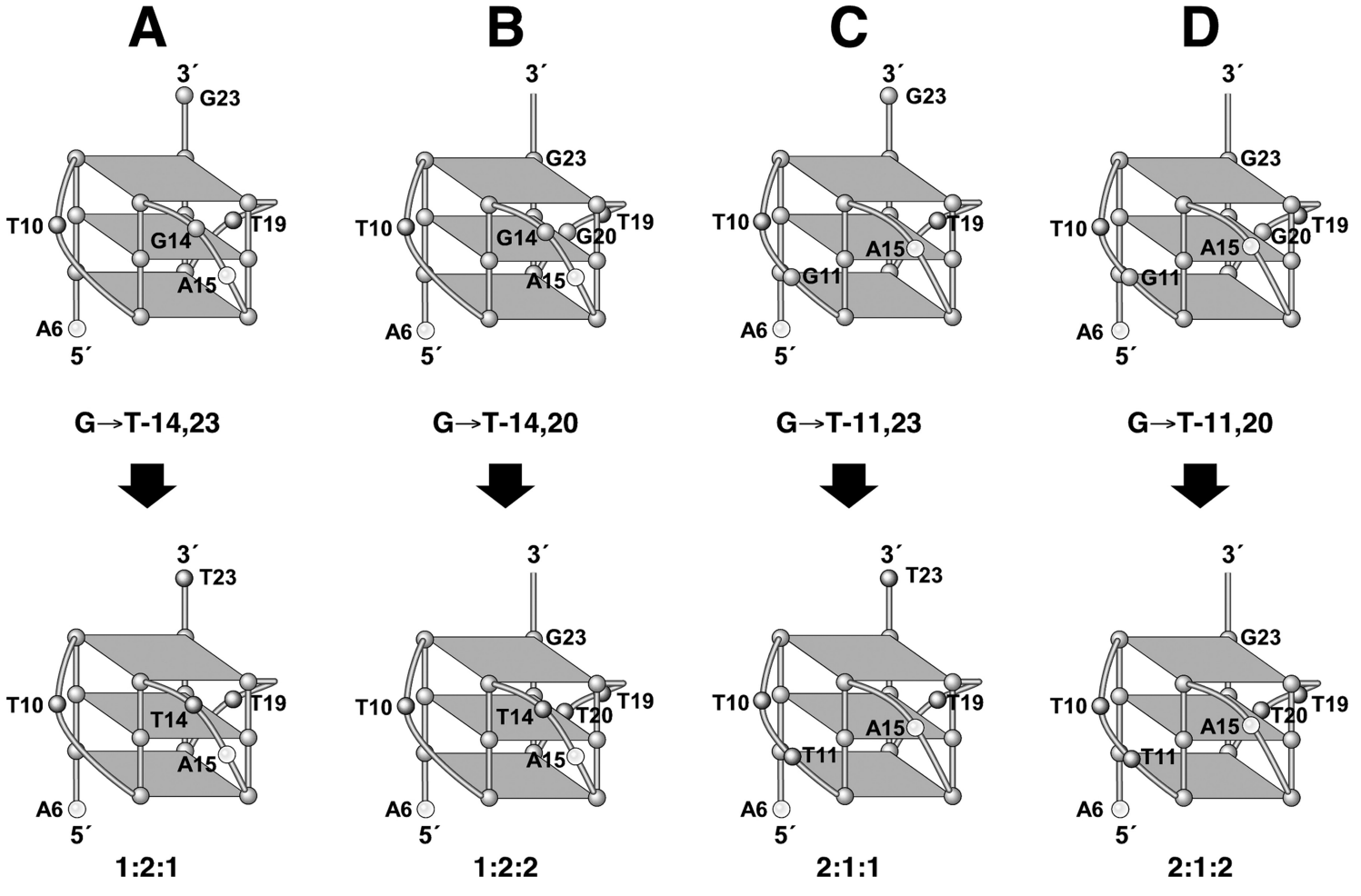

FIGURE 4 (A) Proposed structures of the four different loop isomers, in which dual G-to-T mutations at positions 11, 14, 20, and 23 result in defined loop isomers. The upper row shows the four proposed isomers and the lower row shows the result of dual G-to-T mutations. (B) EMSA of the wild-type (lane 1) and the four Pu18-mer loop isomers (lanes 2–5) containing the dual mutants G→T-14,23, -14,20, -11,23, -11,20, respectively. The Pu18-mer sequence and the positions of the four G-to-T mutations are indicated with asterisks above the EMSA. *(Continued)*

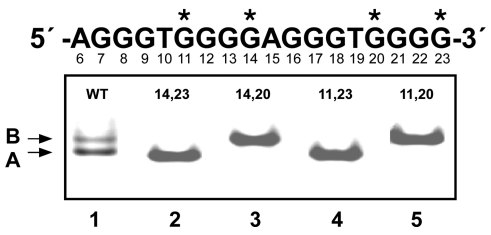

FIGURE 4B (Continued)

mixture. Indeed, the predominance of band A over band B in lane 1 of Figure 4B also supports this conclusion.

Molecular Modeling of the Predominant 1:2:1 Loop Isomer for the Pu18-Mer

The predominant c-MYC G-quadruplex parallel-type structure having the 1:2:1 arrangement of loops (two single-base loops and one loop with two bases, see Figure 4A) was found to be stable during molecular minimization and dynamics calculations (Figure 5). All the guanine bases of the tetrads exist in *anti* conformation. Single-base loops connecting parallel guanine strands were found to be stable, as well as all guanine bases of the strands connected by single-base loops in the tetrad arrangement.

The Parallel G-Quadruplex Is the Repressor Element in the NHE III_1

To evaluate the potential biological significance of the G-quadruplex structures in the NHE III_1, single- or double-base mutations of Pu27 were

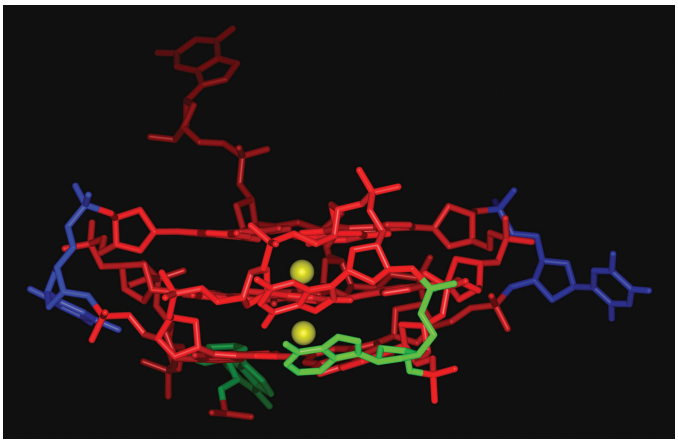

FIGURE 5 Most stable low energy structure of the c-MYC Pu18-mer parallel quadruplex (color coding: adenine = green, cytosine = yellow, guanine = red, thymine = blue) with potassium atoms (as CPK model). For clarity, hydrogen atoms have not been shown.

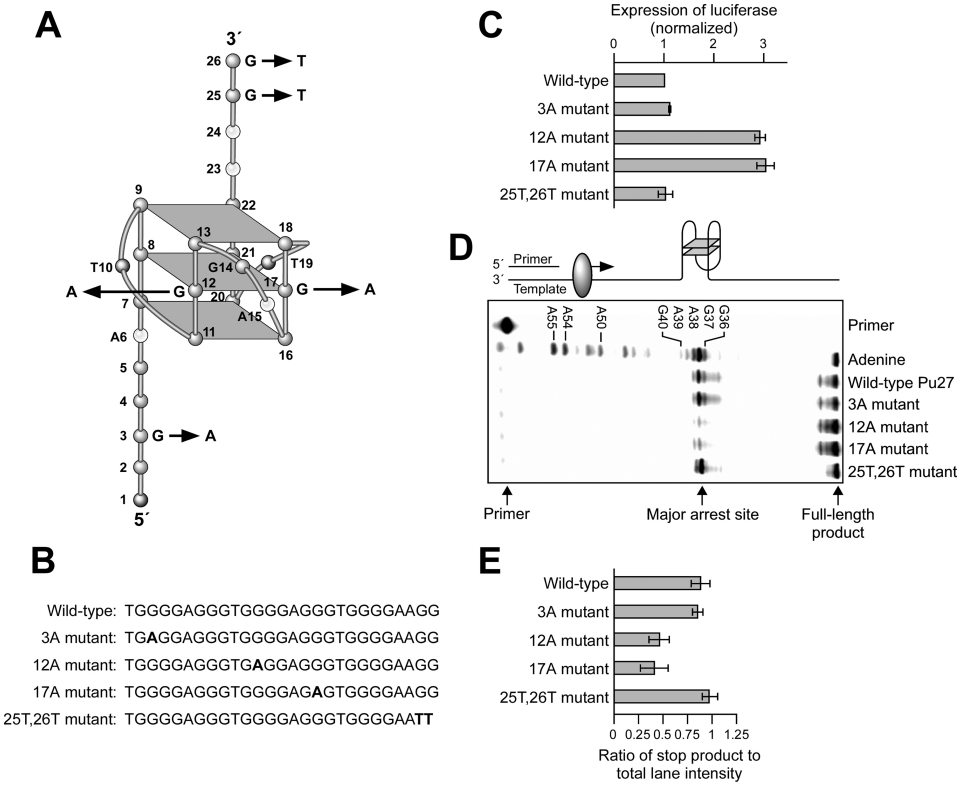

FIGURE 6 Effect of mutations of Pu27 on transcriptional activity and stability of the G-quadruplexes.[22] (A) Cartoon showing the mutations in the parallel G-quadruplex and flanking regions. The positions of the mutants in the G-quadruplex regions are shown by the arrows. (B) The sequences of the Pu26 wild-type (WT) and mutants (3A, 12A, 17A, and 25T, 26T) used in this study. Bases in bold indicate the sites of mutation. (C) Expression of luciferase normalized to the wild-type and various mutant sequences shown in (A). Each data point is the average of three experiments. (D) Polymerase stop assay[33] for determination of the effect of mutations on the stability of the G-quadruplex structure at 45°C in the presence of 10 mM KCl. Each data point is the average of three experiments. The cartoon above the gel illustrates the principle of the assay. The G-quadruplex structure is shown in proximity to the pause site for Taq polymerase. (E) Quantitation of the results from the polymerase stop assay shown in (D).

designed (Figure 6, A and B) and the various constructs were evaluated for both promoter activity in a luciferase reporter assay (Figure 6C) and for the ability to form G-quadruplex structures using a Taq polymerase stop assay (Figure 6, D and E).[28] Four different mutant templates were prepared (see Figure 6, A and B). Three were single-base mutations (G-to-A or G-to-T mutations) either within the central tetrad (positions 12 and 17) or in the 5′ run of four guanines (position 3), which is outside the G-quadruplex region. As a control, a fourth dual mutant template (25,26 G-to-T) was prepared on the 3′ side of the runs of guanine. The two single G-to-A mutations in the central tetrads (positions 12 and 17) caused

a threefold increase in transcriptional activation, while the two mutant templates outside the parallel G-quadruplex structure had a negligible effect. These results suggest that the G-quadruplex structure is a silencer element, since disruption causes an increase in transcriptional activity. The same wild-type and mutant sequences of the Pu27 were used in a Taq polymerase stop assay,[33] which can be used to evaluate the ability of a DNA sequence to form stable G-quadruplex structures. In this assay (Figure 6D), primer extension using Taq polymerase leads to premature stops at G-quadruplex structures. The results show that significant arrest occurs with the wild-type insert at 45°C. The primary arrest site occurs at G37, which corresponds to G7 in Pu27. The two single-base mutations in the central tetrad lead to the loss of G-quadruplex-mediated polymerase arrest, while the mutants outside the G-quadruplex have no effect on the stability of the parallel-stranded G-quadruplex structure (Figure 6, D and E). This result is exactly complementary to that found in the promoter assay in which only those mutations that result in destabilization of the G-quadruplex structure result in enhancement of c-MYC transcriptional activation. Thus, we can conclude that the parallel G-quadruplex is a silencer element in the NHE III_1 of the c-MYC promoter.

All Four Dual Mutant Loop Isomers Are Biologically Relevant to c-MYC Transcriptional Control

G-to-A mutations at either G12 or G17 of the Pu27-mer resulted in a transcriptional activation of about threefold using a luciferase reporter assay.[22] In order to evaluate the transcriptional repressor role of each of the four loop isomers (see Figure 4A), the same dual mutants that dictate the individual loop isomers were evaluated for their effect on transcriptional activation using the same luciferase reporter system. In each case, an increase in basal gene expression of about 2.2–2.4 was seen (see Figure 7), implicating a role for a mixture of the loop isomers in stabilization of the parallel G-quadruplex structure. Mutation of all four guanines involved in the isomeric transitions (i.e., G11, G14, G20, and G23) produced a fivefold increase in basal gene expression, further establishing the importance of these guanines in stabilization of the parallel G-quadruplex structure. Therefore, all four parallel-loop isomers contribute to the stability of the silencer element in the NHE III_1 of the c-MYC promoter. Each dual-mutation isomer was found to contribute to a >twofold increase in basal transcriptional activity. We propose it is this dynamic equilibrium between the loop isomers that provides the entropy and, thus, the stability (T_m = 85°C) of this G-quadruplex structure. This proposal is further supported by the observation that each of the four dual isomers has a significantly lower (about 15°C) melting temperature than the wild-type sequence.

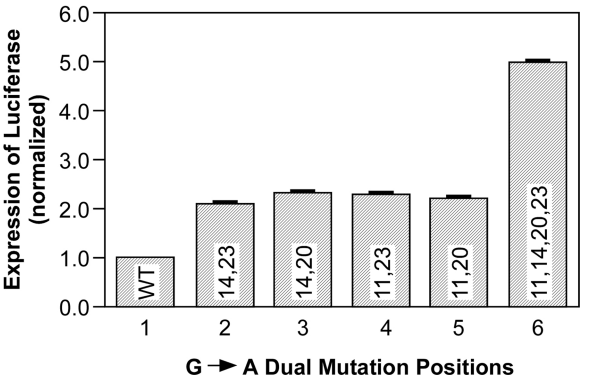

FIGURE 7 Effect of the four dual-loop mutants G→A-14,23, -14,20, -11,23, and -11,20 (lanes 2–5, respectively) and tetra mutant (lane 6) on luciferase expression relative to the wild-type sequence (lane 1). The values are the average of three experiments. The wild-type sequence was assigned a nominal value of 1.0.

NMR Studies Show That a 22-Mer Containing the Biologically Relevant Four 3′-Guanine Runs in the NHE III$_1$ Forms an Intramolecular Propeller-Type Parallel-Stranded G-Quadruplex

The parallel-stranded G-quadruplex topology has been unequivocally determined by a recent NMR spectroscopic study,[34] by using a 22-mer sequence (MYC22) that was expanded from the Pu18 (Figure 8A). Guanine imino protons were assigned unambiguously to their position in the sequence by the site-specific low-enrichment approach using 2% ^{15}N-labled samples. The assignments of guanine H8 protons were obtained by through-bond correlation with the already assigned imino protons via ^{13}C5 at natural abundance. The G-tetrad alignments were determined by the inter-residue connectivities of H8 and H1 protons in NOESY spectra. In a G-tetrad plane, the base H8 of one guanine is in close spatial vicinity to the imino H1 of the adjacent guanine due to the Hoogsteen H-bond network of the G-tetrad (Figure 8B) and their NOE connectivities can be detected. The through-space H8/H1 connectivities define the alignment of a tetrad plane. Once the G-tetrad alignments were determined, the folding topology of the intramolecular G-quadruplex can be defined by connecting sequential residues. This procedure reveals the formation of an intramolecular propeller-type parallel-stranded G-quadruplex, as shown in Figure 8C.

Structure Analysis of the Predominant 22-Mer c-MYC G-Quadruplex Dual Loop Isomer

For NMR structure determination, a sequence with dual G-to-T mutations at positions 14 and 23, which had been shown to isolate the predominant conformation, together with the proper extensions of

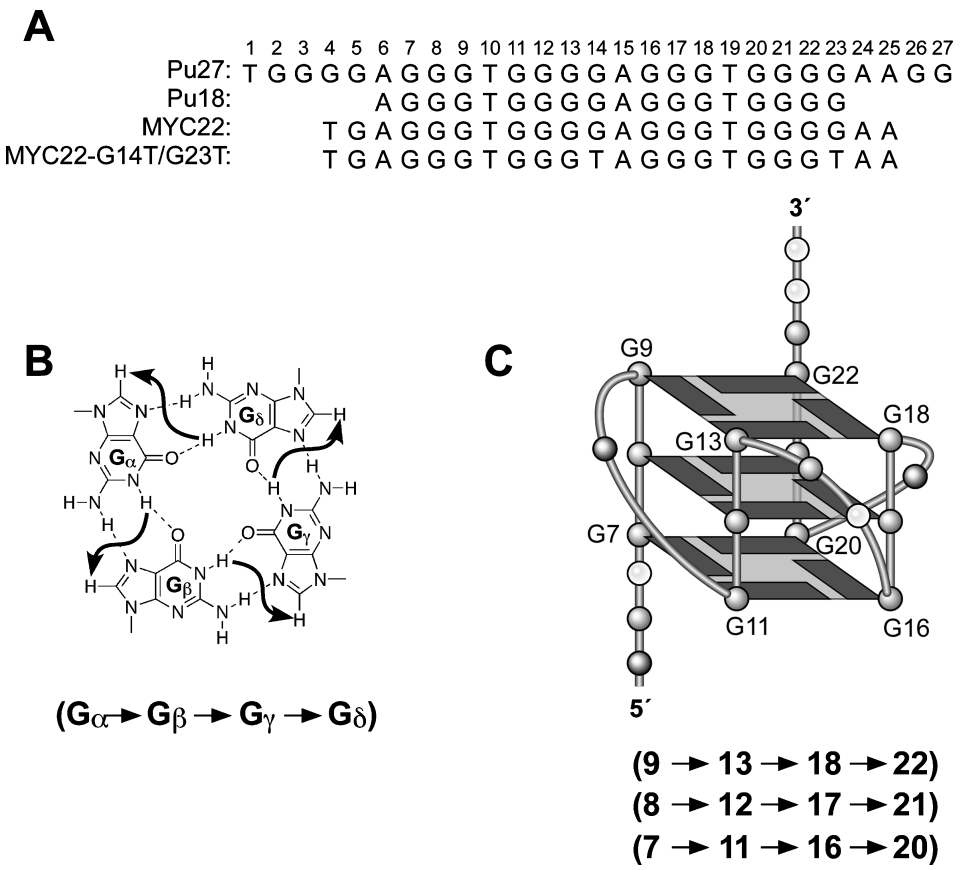

FIGURE 8 (A) The promoter sequence of the c-MYC gene and its modifications. Pu27 is the 27-mer wild-type sequence, Pu18 contains only the necessary G-runs for quadruplex formation, MYC22 is the extended Pu18 sequence that adopts one major parallel structure, and MYC22-G14T/G23T represents the sequence that was used for the solution structure. The numbering system is shown above Pu27. (B) Specific imino–H8 connectivity pattern around a G-tetrad ($G_\alpha \cdot G_\beta \cdot G_\gamma \cdot G_\delta$) indicated with arrows (connectivity between G_δ and G_α implied). (C) Schematic structure of MYC22 that satisfies NOE connectivities shown in parentheses.

the Pu18 that can stabilize the G-quadruplex structure,[35] was designed (MYC22-G14T/G23T, Figure 8A). This oligomer forms a single G-quadruplex structure in K^+ solution at pH 7, as demonstrated by an NMR spectroscopic study.[35] The 1D NMR spectrum of this 14,23-G-to-T mutant c-MYC sequence (MYC22-G14T/G23T) in potassium solution shows significantly improved line width and better resolution compared to that of MYC22.

The quanine imino and base HB protons of MYC22-G14T/G23T were unambiguously assigned by the site-specific incorporation of 1,2,7,-^{15}N, 2-^{13}C-labeled quanine nucleosides at each quanine position of the sequence. The complete proton NMR assignments were made using standard techniques. In accord with the wild-type topology,[28,34] MYC22-G14T/G23T adopts a parallel-stranded G-quadruplex with 1:2:1 side loops of T, TA, and

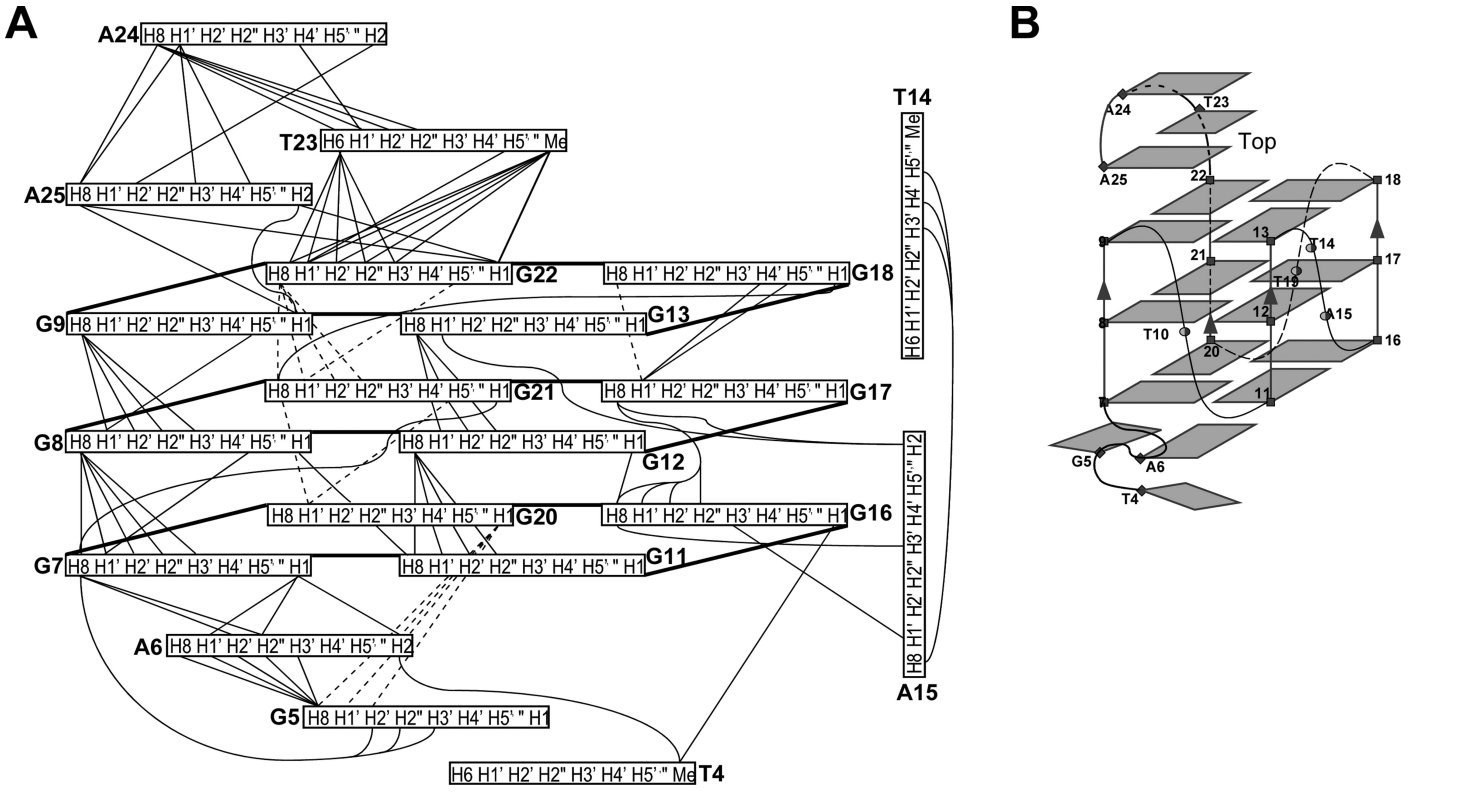

FIGURE 9 Schematic diagram of inter-residue NOE connectivities of the MYC22-G14T/G23T G-quadruplex. Connectivities of the 3′-(T23-A24-A25) and 5′-(T4-G5-A6) extensions and one double-nucleotide side loop (T14A15) are shown by both solid lines and dashed lines. The NOE connectivities clearly define the quadruplex conformation and provide distance restraints for structure calculation.

T, respectively. As previously demonstrated,[34] all of the glycosidic torsion angles of all nucleotides are in the *anti* conformation.

Many inter-residue NOE crosspeaks are observed in 2D-NOESY and are summarized in Figure 9A. These inter-residue NOEs clearly determined the overall structure of the G-quadruplex. NOE connectivities of the G-tetrad guanines show that the three G-tetrads are connected by four parallel right-handed guanine strands. The guanines on each of the four strands connecting three tetrads are very well stacked, as indicated by the clear NOE connections of adjacent guanines (Figure 9A). The topology of the MYC22-G14T/G23T, including the flanking caps, is shown in Figure 9B.

NMR-Restrained Solution Structure of the Predominant 22-Mer c-MYC G-Quadruplex

The starting model of MYC22-G14T/G23T for NOE-restrained structure calculation was constructed based on the aforementioned molecular model (Figure 6) with additional 5′- and 3′-external flanking sequences and modified side loops.[35] A total of 246 distance restraints, of which 61 are from inter-residue NOE interactions, were incorporated into the NOE-restrained molecular dynamics (RMD) calculation with potassium counter ions and water solvent. The RMD calculation produced a family of refined structures, with the average rms deviation being 0.88 Å including all atoms for the 20 lowest energy structures. A representative model of the MYC22-G14T/G23T G-quadruplex structure is shown in two different views in Figure 10, A and B. The G-quadruplex consists of three G-tetrads with four parallel DNA strands that are linked by three double-chain reversal side loops. This is the first example of a parallel G-quadruplex with single-nucleotide, double-chain reversal loops, which appears to be very stable.

Both the 3′- and 5′-flanking sequences form a stable conformation capping the top and bottom ends of the MYC22-G14T/G23T G-quadruplex structure (Figure 10C). The 3′-flanking TAA adopts a well-defined fold-back structure, stacking with the G-tetrad (Figure 10D). The 5′-TGA flanking sequence adopts a more or less left-handed twist backbone conformation, stacking with the bottom G-tetrad (Figure 10E).

The Predominant 22-Mer c-MYC G-Quadruplex Structure Is Very Stable

One-dimensional proton spectra of MYC22-G14T/G23T at various temperatures indicate that this quadruplex structure is extremely stable.[35] The melting temperature of MYC22-G14T/G23T in 95 mM K^+ is over 85°C and cannot be measured by the NMR technique. Even at 85°C, the imino resonances of the four guanines from the central tetrad, G8, G12, G17, and G21, are still clearly observable, indicating that the central G-tetrad is still

stably present. The stability of the c-MYC G-quadruplex is further supported by the H_2O-D_2O exchange experiments. The four guanines (G8, G12, G17, and G21) from the central tetrad are extremely stable against exchange from H_2O to D_2O.

The capping effect explains the mechanism by which the addition of extra nucleotides can enhance the stability of the quadruplex structure.

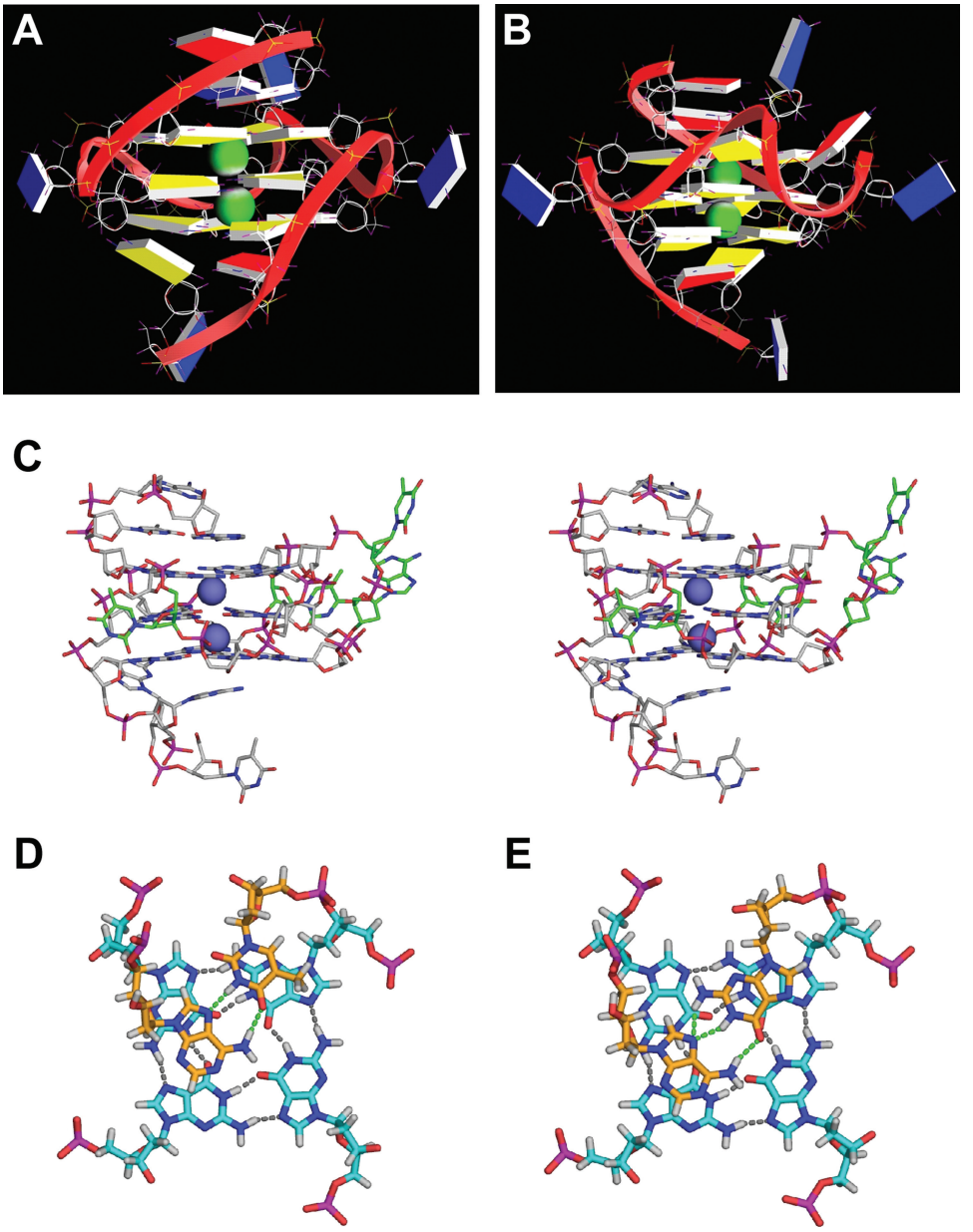

The melting temperature of MYC22-G14T/G23T is over 85°C, very close to the melting temperature of the wild-type Pu27, whereas the melting temperature of Pu18-mer G14T/G23T dual mutant (Figure 4A) is around 70°C (Figure 8A).[28] All these data indicate that our G-quadruplex structure may be biologically relevant, since the wild-type c-MYC promoter DNA, as exemplified by the Pu27-mer, has extended flanking DNA sequences at both ends of the G-rich region and therefore can adopt the needed capping conformations to stabilize the major G-quadruplex conformation. As the Pu27 is located in the intact promoter of c-MYC within a duplex region, it is unlikely that the DNA strands change conformation abruptly from G-quadruplex to duplex structure; therefore, it is highly possible that a transition region, such as the capping structure, can be formed at the junction interface.

SUMMARY AND CONCLUSIONS

On the basis of the studies described in this review, a model for how the parallel G-quadruplex structure acts as a repressor of c-MYC expression can be proposed (Figure 11). CNBP and hnRNP K are single-stranded DNA-binding proteins that activate transcription. The purine-rich strand can be sequestered as a parallel G-quadruplex structure, and this prevents binding of CNBP. It is possible that the pyrimidine-rich strand forms an i-motif structure, which would also prevent hnRNP K binding to this strand. In work not reported here, we have demonstrated that the cationic porphyrin TMPyP4 binds to the parallel G-quadruplex structure to inhibit c-MYC gene expression.[22] Thus, we have demonstrated the principle that c-MYC transcription can be controlled by ligand-mediated G-quadruplex stabilization.

←

FIGURE 10 A representative model of the NMR-refined MYC22-G14T/G23T parallel-stranded G-quadruplex structure in two opposite views, prepared using the program GRASP.[36] Two potassium ions (green spheres) between the G-tetrads are also shown. (A) Viewing from the tetrad groove with no loop. The two flanking sequences capping each end of the G-quadruplex are clearly seen. (B) Viewing from the tetrad groove where the double nucleotide TA loop is located. The two single-T side loops and the double-nucleotide TA loop are clearly seen. Guanine = yellow, adenine = red, thymine = blue. (C) Stereo view showing the double-chain reversal loop structures of the MYC22-G14T/G23T parallel-stranded G-quadruplex. Two potassium ions (blue spheres) between G-tetrads are also shown. Viewing from the first single-T double-chain reversal loop. Nitrogen atoms are blue, oxygen atoms are red, and phosphorus atoms are magenta. Carbon atoms of loop regions are green and the rest of the carbon atoms are gray. (D) and (E) Top views of the G-quadruplex with mutant T23 (D) and wild-type G23 (E). In the MYC22-G14T/G23T double mutant sequence, stacking interactions between the T23:A25 base pair and the top G-tetrad. In the MYC22-G14T sequence, stacking interactions between the wild-type G23:A25 base pair and the top tetrad. The hydrogen bonds of the top tetrad (gray) and the T/G23:A25 base pair (green) are represented in dashed lines. Nitrogen atoms are blue, oxygen atoms are red, phosphorus atoms are magenta, and hydrogen atoms are white. Carbon atoms of the G-tetrad are cyan and carbon atoms of the 3′-flanking sequence are orange.

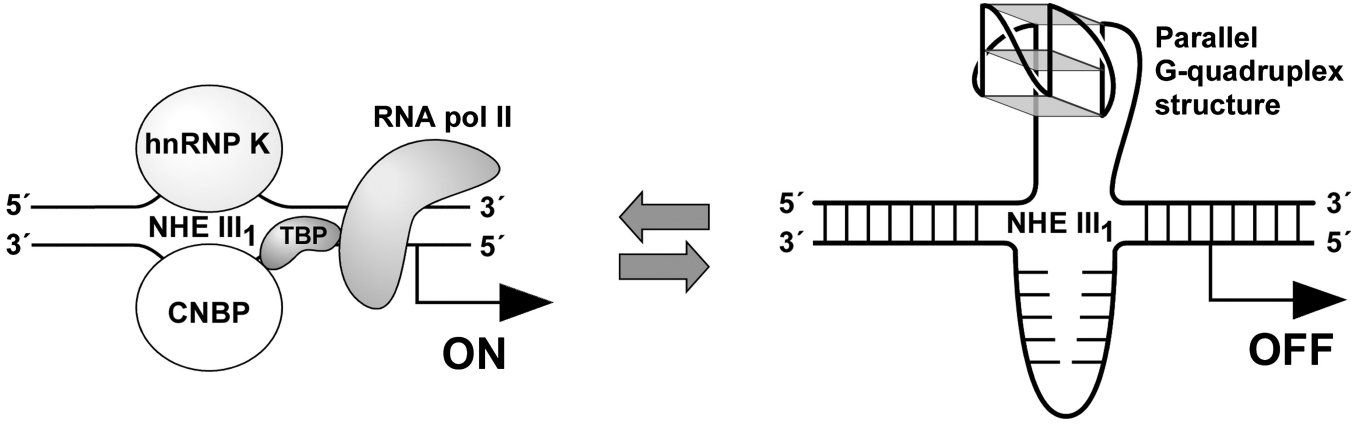

FIGURE 11 Model for the activation and repression of c-MYC gene transcription involving the conversion of the paranemic secondary DNA structures (gene off) to purine and pyrimidine single-stranded DNA forms for transcriptional activation.[22] hnRNP K and CNBP are single-stranded DNA binding proteins involved in transcriptional activation.

REFERENCES

1. Pelengaris, S.; Rudolph, B.; Littlewood, T. Action of MYC In Vivo—Proliferation and Apoptosis. *Current Opinion Genetics and Development* **2000**, 10, 100–105.
2. Spencer, C.A.; Groudine, M. Control of c-MYC Regulation in Normal and Neoplastic Cells. *Advances in Cancer Research* **1991**, 56, 1–48.
3. Marcu, K.B.; Bossone, S.A.; Patel, A.J. MYC Function and Regulation. *Annual Review of Biochemistry* **1992**, 61, 809–860.
4. Facchini, L.M.; Penn, L.Z. The Molecular Role of MYC in Growth and Transformation: Recent Discoveries Lead to New Insights. *FASEB Journal* **1998**, 12, 633–651.
5. Adachi, S.; Obaya, A.J.; Han, Z.; Ramos-Desimone, N.; Wyche, J.H.; Sedivy, J.M. c-MYC Is Necessary for DNA Damage-Induced Apoptosis in the G_2 Phase of the Cell Cycle. *Molecular and Cellular Biology* **2001**, 21, 4929–4937.
6. Canelles, M.; Delgado, M.D.; Hyland, K.M.; Lerga, A.; Richard, C.; Dang, C.V.; Leon, J. Max and Inhibitory c-MYC Mutants Induce Erythroid Differentiation and Resistance to Apoptosis in Human Myeloid Leukemia Cells. *Oncogene* **1997**, 14, 1315–1327.
7. Holt, J.T.; Redner, R.L.; Nienhuis, A.W. An Oligomer Complementary to c-MYC mRNA Inhibits Proliferation of HL-60 Promyelocytic Cells and Induces Differentiation. *Molecular and Cellular Biology* **1988**, 8, 963–973.
8. Prochownik, E.V.; Kukowska, J.; Rodger, C. c-MYC Antisense Transcripts Accelerate Differentiation and Inhibit G1 Progression in Murine Erythroleukemia Cells. *Molecular and Cellular Biology* **1988**, 8, 3683–3695.
9. Jain, M.; Arvanitis, C.; Chu, K.; Dewey, W.; Leonhardt, E.; Trinh, M.; Sundberg, C.D.; Bishop, J.M.; Felsher, D.W. Sustained Loss of a Neoplastic Phenotype by Brief Inactivation of MYC. *Science* **2002**, 297, 102–104.
10. Sakatsume, O.; Tsutsui, H.; Wang, Y.; Gao, H.; Tang, X.; Yamauchi, T.; Murata, T.; Itakura, K.; Yokoyama, K.K. Binding of THZif-1, a MAZ-Like Zinc Finger Protein to the Nuclease-Hypersensitive Element in the Promoter Region of the c-MYC Protooncogene. *Journal of Biological Chemistry* **1996**, 271, 31322–31333.
11. Cooney, M.; Czernuszewicz, G.; Postel, E.H.; Flint, S.J.; Hogan, M.E. Site-Specific Oligonucleotide Binding Represses Transcription of the Human c-MYC Gene In Vitro. *Science* **1988**, 214, 456–459.
12. Siebenlist, U.; Henninghausen, L.; Battey, J.; Leder, P. Chromatin Structure and Protein Binding in the Putative Regulatory Region of the c-MYC Gene in Burkitt Lymphoma. *Cell* **1984**, 37, 381–391.
13. Boles, T.C.; Hogan, M.E. DNA Structure Equilibria in the Human c-MYC Gene. *Biochemistry* **1987**, 26, 367–376.
14. Simonsson, T.; Pribylova, M.; Vorlickova, M. A Nuclease Hypersensitivity Element in the Human c-MYC Promoter Adopts Several Distinct i-Tetraplex Structures. *Biochemical and Biophysical Research Communications* **2000**, 278, 158–166.
15. Simonsson, T.; Pecinka, P.; Kubista, M. DNA Tetraplex Formation in the Control Region of c-MYC. *Nucleic Acids Research* **1998**, 26, 1167–1172.
16. Ji, L.; Arcinas, M.; Boxer, L.M. The Transcription Factor, Nm23H2, Binds to and Activates the Translocated c-MYC Allele in Burkitt's Lymphoma. *Journal of Biological Chemistry* **1995**, 270, 13392–13398.
17. Tomonaga, T.; Levens, D. Activating Transcription from Single Stranded DNA. *Proceedings National Academy of Sciences USA* **1996**, 93, 5830–5835.
18. Bossone, S.A.; Asselin, C.; Patel, A.J.; Marcu, K.B. MAZ, a Zinc Finger Protein, Binds to c-MYC and C2 Gene Sequences Regulating Transcriptional Initiation and Termination. *Proceedings of the National Academy of Sciences USA* **1992**, 89, 7452–7456.
19. Michelotti, E.F.; Tomonaga, T.; Krutzsch, H.; Levens, D. Cellular Nucleic Acid Binding Protein Regulates the CT Element of the Human c-MYC Protooncogene. *Journal of Biological Chemistry* **1995**, 270, 9494–9499.
20. Postel, E.H.; Berberich, S.J.; Rooney, J.W.; Kaetzel, D.M. Human NM23/Nucleoside Diphosphate Kinase Regulates Gene Expression through DNA Binding to Nuclease-Hypersensitive Transcriptional Elements. *Journal of Bioenergetics and Biomembranes* **2000**, 32, 277–284.
21. Collins, I.; Weber, A.; Levens, D. Transcriptional Consequences of Topoisomerase Inhibition. *Molecular and Cellular Biology* **2001**, 21, 8437–8451.

22. Siddiqui-Jain, A.; Grand, C.L.; Bearss, D.J.; Hurley, L.H. Direct Evidence for a G-Quadruplex in a Promoter Region and Its Targeting with a Small Molecule to Repress c-MYC Transcription. *Proceedings of the National Academy of Sciences USA* **2002**, 99, 11593–11598.
23. Schultze, P.; Macaya, R.F.; Feigon, J. Three-Dimensional Solution Structure of the Thrombin-Binding DNA Aptamer d(GGTTGGTGTGGTTGG). *Journal of Molecular Biology* **1994**, 235, 1532–1547.
24. Kelly, J.A.; Feigon, J.; Yeates, T.O. Reconciliation of the X-Ray and NMR Structures of the Thrombin-Binding Aptamer d(GGTTGGTGTGGTTGG). *Journal of Molecular Biology* **1996**, 256, 417–422.
25. Jing, N.J.; Gao, X.L.; Rando, R.F.; Hogan, M.E. Potassium-Induced Loop Conformational Transition of a Potent Anti-HIV Oligonucleotide. *Journal of Biomolecular Structure and Dynanics* **1997**, 15, 573–585.
26. Jing, N.J.; Hogan, M.E. Structure–Activity of Tetrad-Forming Oligonucleotides as a Potent Anti-HIV Therapeutic Drug. *Journal of Biological Chemistry* **1998**, 273, 34992–34999.
27. Padmanabhan, K.; Padmanabhan, K.P.; Ferraras, J.D.; Sadler, J.E.; Tulinsky, A. The Structure of α-Thrombin Inhibited by a 15-MER Single-Stranded DNA Aptamer. *Journal of Biological Chemistry* **1993**, 268, 17651–17654.
28. Seenisamy, J.; Rezler, E.M.; Gokhale, V.; Siddiqui-Jain, A.; Tye, D.; Powell, T.J.; Hurley, L.H. The Dynamic Character of the G-Quadruplex Element in the c-MYC Promoter and the Product upon Modification by TMPyP4. *Journal of the American Chemical Society* **2004**, 126, 8702–8709.
29. Dapic, V.; Abdomerovic, V.; Marrington, R.; Peberdy, J.; Rodger, A.; Trent, J.O.; Bates, P.J. Biophysical and Biological Properties of Quadruplex Oligodeoxyribonucleotides. *Nucleic Acids Research* **2003**, 31, 2097–2107.
30. Kettani, A.; Gorin, A.; Majumdar, A.; Hermann, T.; Skripkin, E.; Zhao, H.; Jones, R.; Patel, D.J. A Dimeric DNA Interface Stabilized by Stacked A·(G·G·G·G)·A Hexads and Coordinated Monovalent Cations. *Journal of Molecular Biology* **2000**, 297, 627–644.
31. Matsugami, A.; Okuizumi, T.; Uesugi, S.; Katahira, M. Intramolecular Higher Order Packing of Parallel Quadruplexes Comprising a G:G:G:G Tetrad and a G(:A):G(:A):G(:A):G Heptad of GGA Triplet Repeat DNA. *Journal of Biological Chemistry* **2003**, 278, 28147–28153.
32. Matsugami, A.; Ouhashi, K.; Kanagawa, M.; Liu, H.; Kanagawa, S.; Uesugi, S.; Katahira, M. An Intramolecular Quadruplex of $(GGA)^4$ Triplet Repeat DNA with a G:G:G:G Tetrad and a G(:A):G(:A):G(:A):G Heptad, and Its Dimeric Interaction. *Journal of Molecular Biology* **2001**, 313, 255–269.
33. Han, H.; Salazar, M.; Hurley, L.H. A DNA Polymerase Stop Assay for G-Quadruplex-Interactive Compounds. *Nucleic Acids Research* **1999**, 27, 537–542.
34. Phan, A.T.; Modi, Y.S.; Patel, D.J. Propeller-Type Parallel-Stranded G-Quadruplexes in the Human c-MYC Promoter. *Journal of the American Chemical Society* **2004**, 126, 8710–8716.
35. Ambrus, A.; Chen, D.; Dai, J.; Jones, R.A.; Yang, D. Solution Structure of the Biologically Relevant G-Quadruplex Element in the Human c-MYC Promoter. Implications for G-Quadruplex Stabilization. *Biochemistry* **2004**, 44, 2048–2058.
36. Nicholls, A.; Sharp, K.A.; Honig, G. Protein Folding and Association: Insights from the Interfacial and Thermodynamic Properties of Hydrocarbons. *Proteins: Structure, Function and Genetics* **1991**, 11, 281–296.